crystals

MDPI

Article

Perovskite Quantum Dot/Zinc Oxide Composite Films for Enhanced Luminance

Nikita Khairnar †, Hyukmin Kwon †, Sunwoo Park †, Sangwook Park, Hayoon Lee and Jongwook Park *

Integrated Engineering, Department of Chemical Engineering, Kyung Hee University, Yongin-si 17104, Republic of Korea

* Correspondence: jongpark@khu.ac.kr; Tel.: +82-10-8759-8485

† These authors contributed equally to this work.

Abstract: We conducted experiments utilizing the scattering effect of zinc oxide (ZnO) to enhance the photoluminescence (PL) intensity of cesium lead bromide ($CsPbBr_3$) perovskite quantum dots (QDs). This study involved investigating the method for creating a $CsPbBr_3$ and ZnO mixture and determining the optimal mixing ratio. A mixture dispersion of $CsPbBr_3$ and ZnO, prepared at a 1:0.015 weight ratio through shaking, was fabricated into a film using the spin coating method. The PL intensity of this film showed a relative increase of 20% compared to the original $CsPbBr_3$ QD film without ZnO. The scattering effect of ZnO was confirmed through ultraviolet-visible (UV-Vis) absorption and transient PL experiments, and a long-delayed exciton lifetime was observed in the optimized mixture dispersion thin film. The morphology of the fabricated film was characterized using field emission scanning electron microscopy (FESEM), transmission electron microscopy (TEM), and atomic force microscopy (AFM). For the $CsPbBr_3$-ZnO mixture (1:0.0015) film, crystal domains of approximately 10 nm were observed using TEM. Through AFM analysis, an excellent film roughness of 4.6 nm was observed, further confirming the potential of perovskite QD/ZnO composite films as promising materials for enhanced photoconversion intensity. In future studies, applying this method to other perovskite materials and metal oxides for the optimization of photoconversion composite materials is expected to enable the fabrication of highly efficient perovskite QD/metal oxide composite films.

Keywords: perovskite quantum dots; metal oxide; ZnO; light scattering

Citation: Khairnar, N.; Kwon, H.; Park, S.; Park, S.; Lee, H.; Park, J. Perovskite Quantum Dot/Zinc Oxide Composite Films for Enhanced Luminance. *Crystals* **2024**, *14*, 937. https://doi.org/10.3390/cryst14110937

Academic Editor: Francisco M. Morales

Received: 17 October 2024
Revised: 27 October 2024
Accepted: 28 October 2024
Published: 29 October 2024

1. Introduction

Halide perovskites are primarily classified into two main types: one is the organic–inorganic hybrid type ($APbX_3$, where A represents methyl ammonium compounds and X represents halides such as Br, I, or Cl), and the other is the inorganic perovskite type (e.g., $CsPbX_3$) [1–5]. While organic–inorganic hybrids are preferred due to their cost-effectiveness, facilitated by efficient synthesis methods at ambient temperatures, inorganic perovskites like cesium lead bromide ($CsPbBr_3$) often require high-temperature processing above 150 °C [6]. However, they offer advantageous material stability and superior thermal stability, ensuring reliable performance under high-temperature conditions, which provides commercial advantages in terms of storage stability and material reliability [7,8]. Consequently, these robust characteristics can address the drawbacks of organic–inorganic perovskite materials, which are easily degraded by moisture and heat. In particular, $CsPbX_3$ offers optical advantages, including color tuning of the emission wavelength depending on the type of halide, narrow full width at half maximum (FWHM) of the emission characteristics, and the ability to achieve high photoluminescence quantum yield (PLQY). Due to these properties, $CsPbX_3$ has attracted significant interest as a promising candidate electronic material for various high-performance optoelectronic devices, including photoconversion films, light-emitting diodes (LEDs), lasers, and photodetectors [1,9–13]. Recent advancements in perovskite photoconversion films and LED technology have primarily focused on

enhancing the PLQY by reducing non-radiative recombination losses, making it a key area of research and development. Non-radiative recombination can occur due to surface defects and low-charge carrier mobility. To address these issues, there is active research on surface engineering techniques based on additives for improving surface defects and dimension engineering. For example, introducing potassium bromide (KBr) into the perovskite film can lead to the passivation of dangling bonds at the bond sites of bromine-deficient Pb, thereby improving the photoconversion efficiency. In cases where such defects are not passivated, they typically capture carriers. However, when these defects are passivated, the PLQY can increase from 66% to 95%. Additionally, applying this method in perovskite light-emitting diode (PeLED) devices can enhance the external quantum efficiency (EQE) to 21% [14]. In addition to these approaches, methods for increasing PLQY through the light-scattering effect of metal oxides have also been proposed. Park et al. demonstrated that high-refractive-index nanoparticles such as TiO_2 and Y_2O_3-ZrO_2 can function as scattering layers in organic light-emitting diode (OLED) devices, improving light extraction efficiency without compromising display quality [15]. Furthermore, a new approach has been proposed by our group to improve perovskite efficiency by utilizing the light-scattering effect of metal oxides. It was reported that incorporating SiO_2 with a refractive index of 1.46 and Al_2O_3 with a refractive index of 1.76 into the perovskite quantum dot (QD) film resulted in an enhancement in photoconversion efficiency by 1.3 to 1.4 times [16]. This phenomenon can be interpreted as the repeated scattering of light occurring within the film, where the cumulative scattering effects enable the perovskite emitters to exhibit relatively high photoluminescence (PL). Among metal oxides, zinc oxide (ZnO), which has a refractive index of 2.0, exhibits superior thermal stability, as well as low costs and environmentally friendly properties, making it a highly promising material for various optoelectronic applications [17–22]. However, ZnO becomes highly fragile upon exposure to acidic or basic environments. Utilizing these characteristics of ZnO, Jha et al. explored the scattering effects occurring in ZnO films and confirmed that ionized impurities and charge defects serve as primary scattering centers influencing charge mobility and bandgap transitions [23]. From these results, research on semiconductor materials such as ZnO has demonstrated how scattering mechanisms can be utilized to enhance device performance in various optoelectronic applications [24–29]. Therefore, this study aims to optimize the fabrication of thin films by dispersing ZnO into $CsPbBr_3$-based perovskite QDs and to evaluate the applicability of the photoconversion films through optical characterization and morphological analysis.

2. Materials and Methods

2.1. General Information

All chemicals were used without further purification. Cesium carbonate (Cs_2CO_3, 99%), lead (II) bromide ($PbBr_2 \geq 98\%$), 1-octadecene (ODE, 90%), oleylamine (OAm, 70%), octane anhydrous (≥99%), methyl acetate (MeOAc, 95%, anhydrous), and Ethyl alcohol (99.9%, anhydrous) were purchased from Sigma-Aldrich. ZnO (Avantama N-10) was purchased from Avantama AG in Switzerland. Acetone, ethanol, deionized water, and isopropyl alcohol used for washing the glass were of HPLC grade with a high purity of >99.9%, and these solvents were purchased from SAMCHUN Chemicals (Seoul, Republic of Korea). The washed glass was additionally cleaned with a UV Ozone cleaner (JAESUNG Engineering, Anyang, Republic of Korea). An ultrasonic digital cleaner (SAEHAN Ultrasonic Co., Seoul, Republic of Korea) was used during the washing of the glass for film fabrication, as well as to mix the perovskite solution and ZnO dispersion. A vortex mixer (KMC-1300V) was used for shaking (VISION Co., Daejeon, Republic of Korea). Spin-coated films were fabricated with a spin coater (SPIN 1200, MIDAS System, Daejeon, Republic of Korea).

Field emission scanning electron microscopy (FESEM) images were obtained using a JSM-7900F instrument (JEOL, Tokyo, Japan). Transmission electron microscopy (TEM) images were obtained using a Tecnai G2 F30 S-Twin (FEI, Hillsborough, OR, USA). The particle sizes were determined using ImageJ software (version 1.54d). ImageJ is a Java-

based, multithreaded, freely available, open-source, platform-independent, and public domain program for image processing and analysis. It was developed at the National Institutes of Health in the USA. Optical ultraviolet-visible (UV-Vis) absorption spectra were obtained using a UV-1900i UV/Vis/NIR spectrometer (Shimadzu, Kyoto, Japan). A Perkin-Elmer LS55 (Xenon flash tube) luminescence spectrometer (PerkinElmer, Waltham, MA, USA) was used to analyze PL spectroscopy. Atomic force microscopy (AFM) images were obtained using a D3100 microscope (Veeco, Plainview, NY, USA). Transient PL (TRPL) decay time values were obtained by using Quantaurus Tau (Hamamatsu, Shizuoka, Japan).

2.2. Synthesis of Perovskite

2.2.1. Synthesis of Cs-Oleate Solution

Cs_2CO_3 (0.40 g, 1.25 mmol), ODE (15 mL), and OA (1.25 mL) were loaded into a 50 mL two-neck flask and dried by degassing under vacuum at 120 °C for 1 h. Following this, the mixture was heated at 150 °C under N_2 until a clear solution was obtained. To avoid the precipitation of the resultant Cs-oleate at room temperature, it was heated to a temperature above 100 °C.

2.2.2. Synthesis of Pristine and Passivated $CsPbBr_3$ QDs

$PbBr_2$ (0.564 mmol), ODE (15 mL), OA (1.5 mL), and OAm (1.5 mL) were loaded into a 100 mL three-neck flask and dried by degassing under vacuum at 120 °C for 1 h. Following this, the mixture was heated under N_2 to 180 °C, and the prepared Cs-oleate (2 mL) was quickly injected. After 5 s, the reaction mixture was cooled using an ice bath and centrifuged at 10,000 rpm for 5 min. Subsequently, the resultant precipitate was collected, dispersed in toluene (5 mL) and methyl acetate (5 mL), and centrifuged at 10,000 rpm for 10 min. The resultant precipitate was then redispersed in toluene (10 mL) and centrifuged at 10,000 rpm for 10 min, and the supernatant was collected [30,31].

2.3. Method for Fabricating Films Using the Dispersion

A 1 wt% $CsPbBr_3$ solution was prepared by dissolving 110 mg of $CsPbBr_3$ QD powder in 11 mL of octane. ZnO solutions with concentrations of 0.08, 0.15, 0.3, and 0.5 wt% were prepared from a ZnO solution (Avantama N-10, 2.5 wt% in ethanol). To prepare a 1.1 mL mixed solution, 0.1 mL of each ZnO solution was added to 1 mL of the 1 wt% $CsPbBr_3$ solution. The mixed solution was dispersed using an ultrasonic digital cleaner and a vortex mixer, each for 5 min. Glass substrates (25 mm × 25 mm) were immersed in a tray containing acetone, which was then placed in an ultrasonic digital cleaner for 10 min of washing. The same process was sequentially repeated with ethanol, deionized water, and isopropyl alcohol, and the substrates were dried in an oven at 80 °C for 10 min. The substrates were further cleaned with a UV-ozone cleaner for 10 min prior to spin coating. The resulting solution mixtures were spin-coated onto the cleaned glass substrates at 2000 rpm for 60 s using a spin coater, followed by annealing at 60 °C for 10 min.

3. Results and Discussion

3.1. Preparation of the $CsPbBr_3$-ZnO Mixture Solutions

$CsPbBr_3$-based perovskite nanocrystals are representative perovskite materials known for their green luminescence, featuring a typical 1:1:3 structure formed by the combination of metal cations and halide anions. In this study, the refractive index of metal oxides with superior optical properties was utilized to induce light scattering within the film. By incorporating ZnO, which has a refractive index of 2.0, into the perovskite film, we aimed to enhance the repeated scattering effects within the film, enabling the perovskite emitters to exhibit relatively high PL efficiency. Such attempts were previously reported by our group, where we achieved enhanced efficiency using SiO_2 and Al_2O_3 [16]. Generally, for perovskite materials, the use of polar solvents, such as alcohol, can lead to the dissociation of the perovskite bonds, which may affect the crystalline structure and reduce luminescence efficiency. Furthermore, perovskite materials are sensitive to moisture, and contact with

water can cause the degradation of the crystals, compromising the stability of the material. Consequently, nonpolar solvents, such as octane, are primarily used. However, solutions of metal oxides such as ZnO are typically prepared using polar solvents like alcohol, resulting in the presence of -OH groups on the surface of the metal oxide. It has been reported that ZnO nanocrystals are readily dispersible in bare dimethyl sulfoxide [32]. This creates a polar solution that contrasts with the perovskite, and simple mixing can lead to phase separation, adversely affecting the optical properties of $CsPbBr_3$ and resulting in decreased efficiency. To mitigate these negative factors, this study aimed to produce a dispersion solution during the mixing of the two solutions. We selected appropriate concentrations and compared the results of solution preparation using sonication or shaking after mixing. This dispersion state helps prevent aggregation, allowing for the attainment of uniform thin films prior to fabrication via spin coating. In this study, octane and ethanol were used as good solvents for $CsPbBr_3$ and ZnO, respectively. Before mixing, both solutions were observed to be in a very clear state (Figure 1a). The methods for mixing the two solutions are detailed in Section 2: Materials and Methods. The mixture solution prepared by sonication exhibited a rapid sedimentation of $CsPbBr_3$ crystals immediately after preparation, with noticeable settling occurring within 10 min. After 40 min, the upper solution became transparent, indicating the final separation of the solvent and the crystals (Figure 1b). In contrast, the solution prepared by shaking maintained a dispersed state of $CsPbBr_3$ and ZnO even after 40 min, as shown in Figure 1c. After preparing the solution using sonication and shaking methods, the surface of the spin-coated film was visually confirmed to be clean, as shown in Figure 2(b-1,c-1). Additionally, as observed in Figure 2a–c, exposure to UV light resulted in visible green luminescence from both the solution and the film.

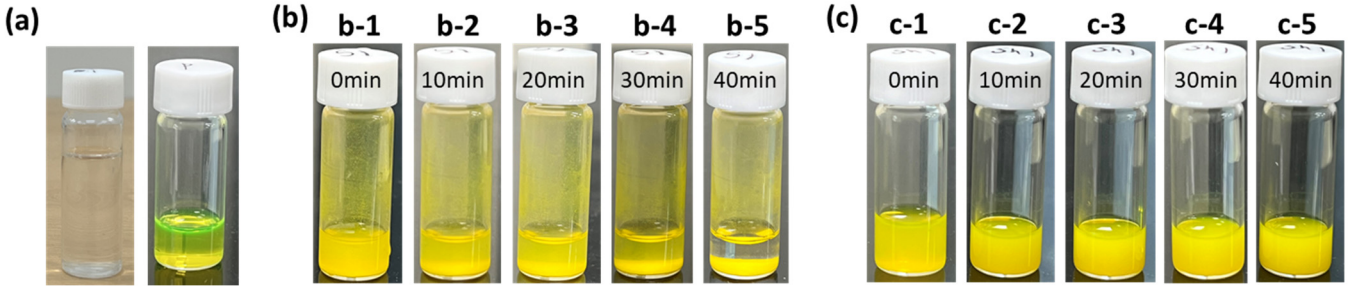

Figure 1. Photos of solutions: (**a**) ZnO (0.15 wt%) in ethanol (**left**) and $CsPbBr_3$ (1 wt%) in octane (**right**); (**b**) $CsPbBr_3$-ZnO (1: 0.015) solutions after sonication; and (**c**) $CsPbBr_3$-ZnO (1: 0.015 wt ratio) solutions after shaking.

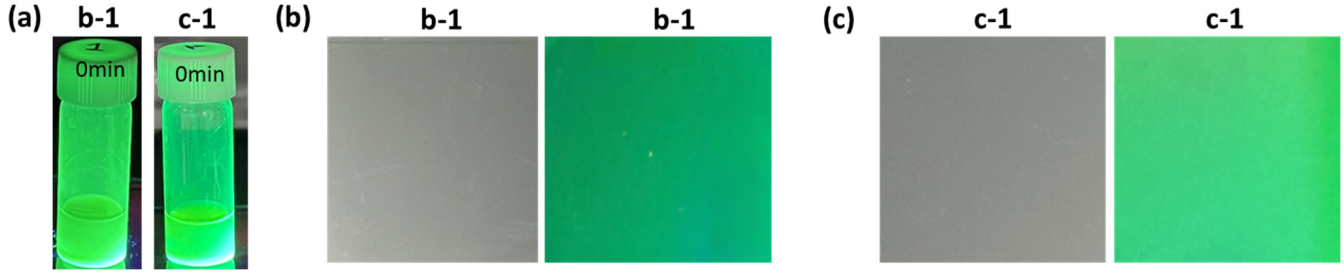

Figure 2. (**a**) Photos of solutions under UV light, (**b**) photos of spin-coated films using sonication without UV light (**left**) and under UV light (**right**), and (**c**) photos of spin-coated films using shaking without UV light (**left**) and under UV light (**right**).

3.2. Photophysical Properties of the $CsPbBr_3$-ZnO Mixture Films

The UV-Vis absorption spectra of the $CsPbBr_3$-ZnO mixture films were measured. The measured UV-Vis properties are summarized in Table 1. It was found that the absorption pattern of $CsPbBr_3$ remained similar even with the inclusion of ZnO (Figure 3). A slight

decrease in intensity was observed, which can be attributed to the dilution effect caused by the presence of ZnO, resulting in a minor reduction compared to the absorption intensity of $CsPbBr_3$. The UV-Vis absorption maximum wavelength (UVmax) of all the prepared $CsPbBr_3$-ZnO mixture films was found to be comparable to that of the original $CsPbBr_3$, measuring at 503 nm. This observation suggests that ZnO, which has an absorption range from 300 to 400 nm, does not interfere with the absorption mechanism of $CsPbBr_3$ and does not form a new excited state.

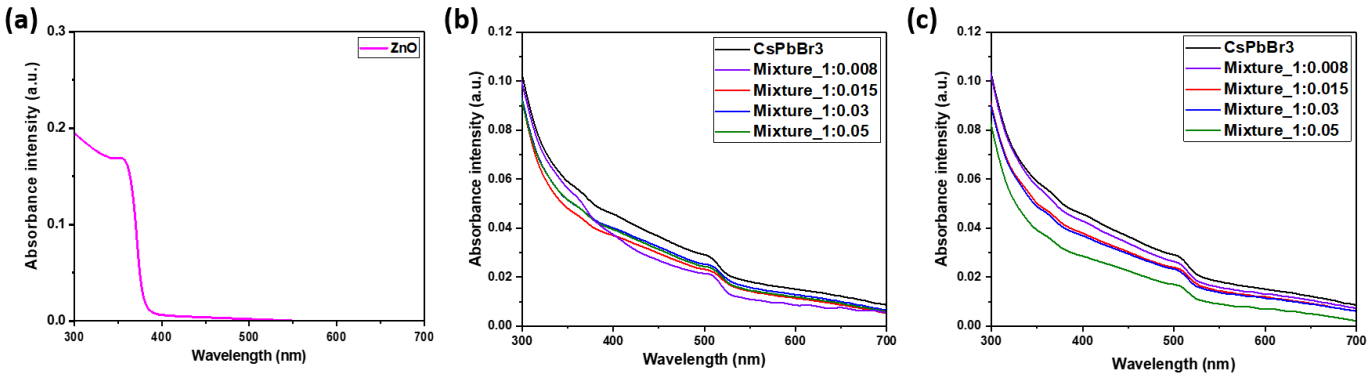

Figure 3. UV-Vis absorption spectra of ZnO, $CsPbBr_3$ and the $CsPbBr_3$-ZnO mixture in the film state: (**a**) ZnO, (**b**) after sonication, and (**c**) after shaking.

Table 1. Maximum wavelength and intensity of UV-Vis absorption for $CsPbBr_3$ and the $CsPbBr_3$-ZnO mixture in the film state.

$CsPbBr_3$ and the Mixture	**Sonication**		**Shaking**	
	λ_{abs} (nm)	**Absorption Intensity**	**λ_{abs} (nm)**	**Absorption Intensity**
$CsPbBr_3$	503	0.029	503	0.029
$CsPbBr_3$-ZnO ratio (1:0.008)	507	0.020	505	0.026
$CsPbBr_3$-ZnO ratio (1:0.015)	507	0.022	504	0.024
$CsPbBr_3$-ZnO ratio (1:0.03)	507	0.025	504	0.022
$CsPbBr_3$-ZnO ratio (1:0.05)	507	0.023	504	0.017

The PL of films made using solutions prepared by sonication and shaking methods was measured, and the PL intensity was compared. The measured PL properties are summarized in Table 2. The results indicated that the shaking method is more effective in maintaining a superior overall PL intensity trend (Figure 4). It is believed that when using sonication, the formation of $CsPbBr_3$ QDs as crystals leads to a decrease in the concentration of $CsPbBr_3$ in the dispersion solution, resulting in lower PL intensity. In addition, when sonication is used instead of shaking, the rapid vibrations may cause the perovskite to quickly precipitate as crystals, leading to self-organization and the formation of larger structures. In this case, the perovskite may shift from a quantum dot form to a bulk type, potentially lowering luminescence efficiency [33]. Further studies are underway. On the other hand, films derived from solutions prepared using the shaking method showed an increase in PL intensity at ratios of 1:0.008 and 1:0.015, measuring 648 and 720, respectively, compared to the intensity of pure $CsPbBr_3$ at 598. However, when the ZnO ratio was further increased, the PL intensity decreased again, indicating that the ratio of 1:0.015 is optimized. As a result, the film made from a $CsPbBr_3$-ZnO solution with a weight ratio of 1:0.015 under shaking method exhibited the highest PL intensity, showing approximately a 20% improvement over the original $CsPbBr_3$. The PL maximum wavelength (PLmax) of $CsPbBr_3$ was 515 nm, while that of ZnO was 385 nm. All mixtures in the film state exhibited PLmax values similar to that of $CsPbBr_3$. This is likely because the PL intensity of ZnO is very weak, and the PL region of ZnO does not overlap with that of $CsPbBr_3$. Furthermore,

since ZnO does not absorb visible light in the 400 nm to 800 nm range, it is interpreted as not affecting the emission of $CsPbBr_3$.

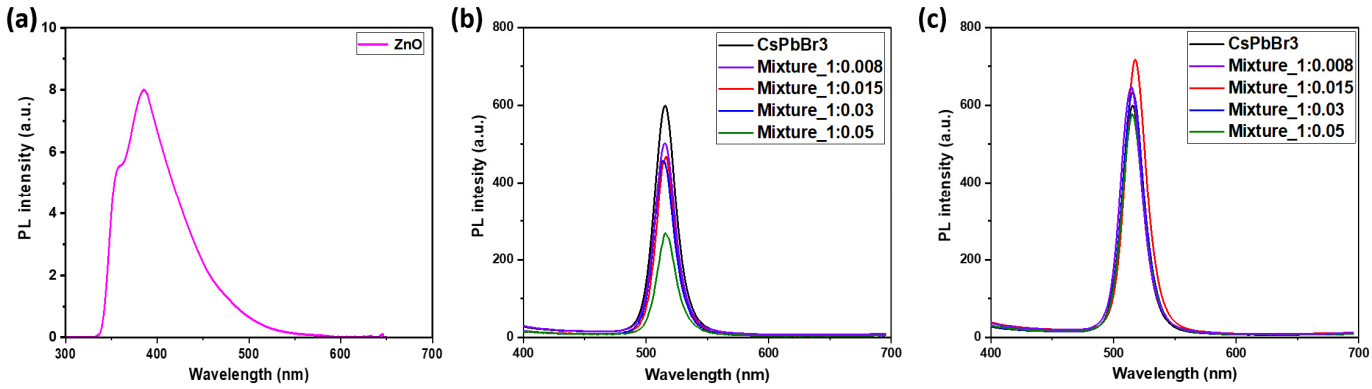

Figure 4. PL spectra of ZnO, $CsPbBr_3$ and the $CsPbBr_3$-ZnO mixture in the film state: (**a**) ZnO, (**b**) after sonication, and (**c**) after shaking.

Table 2. Maximum wavelength and intensity of PL for $CsPbBr_3$ and the $CsPbBr_3$-ZnO mixture in the film state.

$CsPbBr_3$ and the Mixture	**Sonication**		**Shaking**	
	λ_{PL} (nm)	**PL Intensity**	**λ_{PL} (nm)**	**PL Intensity**
$CsPbBr_3$	515	598	515	598
$CsPbBr_3$-ZnO ratio (1:0.008)	515	504	514	648
$CsPbBr_3$-ZnO ratio (1:0.015)	516	468	517	720
$CsPbBr_3$-ZnO ratio (1:0.03)	514	458	515	632
$CsPbBr_3$-ZnO ratio (1:0.05)	515	268	515	576

To investigate the behavior of excited electrons, TRPL was measured on films fabricated under shaking conditions, which showed excellent PL intensity (Figure 5). The measured delayed exciton lifetimes are summarized in Table 3. In this study, the delayed fluorescence lifetime of the $CsPbBr_3$ films was determined to be 74.8 ns, and the x-axis range of the delayed spectrum was displayed up to 3000 ns. The four films with different ZnO mixture ratios exhibited longer delayed lifetimes than $CsPbBr_3$. The $CsPbBr_3$ and ZnO mixture with a 1:0.015 ratio showed the longest delayed lifetime of 81.0 ns. This can be interpreted as the scattering effect induced by ZnO within the perovskite film, which prolongs the emission process and leads to a relatively longer delayed lifetime in the TRPL results. The delayed lifetime started to increase compared to the pristine film at a 1:0.008 ratio, reaching the longest value at a 1:0.015 ratio. Consequently, TRPL measurements confirmed the occurrence of light scattering in $CsPbBr_3$ due to ZnO. The film fabricated under shaking conditions with a $CsPbBr_3$-ZnO weight ratio of 1:0.015 exhibited the highest PL intensity and the longest delayed TRPL lifetime, demonstrating consistency with the optimized ratio.

Table 3. Delayed exciton lifetime of $CsPbBr_3$ and the $CsPbBr_3$-ZnO mixtures in film state.

$CsPbBr_3$ and the Mixtures	**Delayed Exciton Lifetime [a] (ns)**
$CsPbBr_3$	74.8
$CsPbBr_3$-ZnO (1:0.008)	74.5
$CsPbBr_3$-ZnO (1:0.015)	81.0
$CsPbBr_3$-ZnO (1:0.03)	74.3
$CsPbBr_3$-ZnO (1:0.05)	69.5

[a] Calculated by TRPL decay.

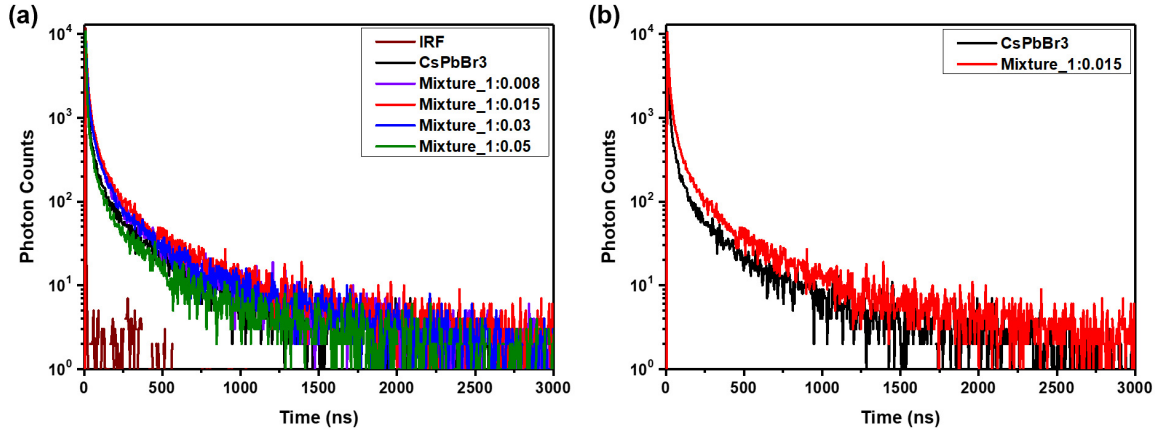

Figure 5. (**a**) TRPL spectra of $CsPbBr_3$ and the $CsPbBr_3$-ZnO mixtures in the film state. (**b**) TRPL spectra of $CsPbBr_3$ and $CsPbBr_3$-ZnO weight ratio of 1:0.015 in the film state.

3.3. Morphology of the $CsPbBr_3$-ZnO Mixture Films

Using FESEM, TEM, and AFM, we compared the morphologies of films derived from the optimized 1:0.015 weight ratio of $CsPbBr_3$-ZnO, which exhibited the best optical properties, with those of pure ZnO and pure $CsPbBr_3$ films. Through this morphological comparison, we assessed the potential for improving light conversion efficiency. Using FESEM analysis, the shapes of ZnO and $CsPbBr_3$ were examined (Figure 6). The $CsPbBr_3$ particles were observed to have a square shape, while the ZnO particles exhibited a rounded shape. The $CsPbBr_3$-ZnO mixture film demonstrated enhanced dispersion and exhibited a relatively dense surface. While vacancies could lead to a reduction in PL efficiency, such possibilities were difficult to identify.

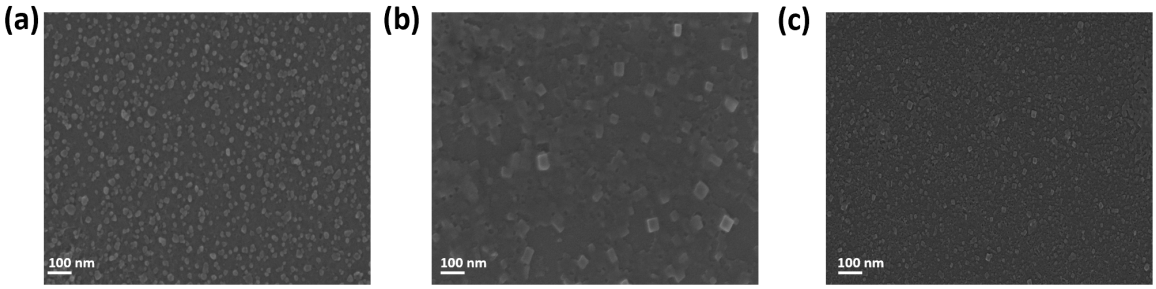

Figure 6. FESEM images of (**a**) ZnO, (**b**) $CsPbBr_3$, and (**c**) the $CsPbBr_3$-ZnO mixture (1:0.015) in the film state.

Further TEM analysis was performed to achieve a more accurate assessment of the morphology (Figure 7). The $CsPbBr_3$ particles presented a rectangular structure that was close to a cubic form [31], while the ZnO particles showed a clearly defined spherical shape. The average particle sizes obtained from the TEM analysis were 10.2 nm for ZnO and 9.55 nm for $CsPbBr_3$, enabling the precise verification of their shapes and dimensions. Figure 7c reveals the presence of randomly arranged ZnO and $CsPbBr_3$ in the $CsPbBr_3$-ZnO mixture (1:0.015) film, allowing for the confirmation of maintained lattice size and arrangement. Consequently, this suggests the potential for improved light conversion efficiency in the $CsPbBr_3$-ZnO mixture (1:0.015) film.

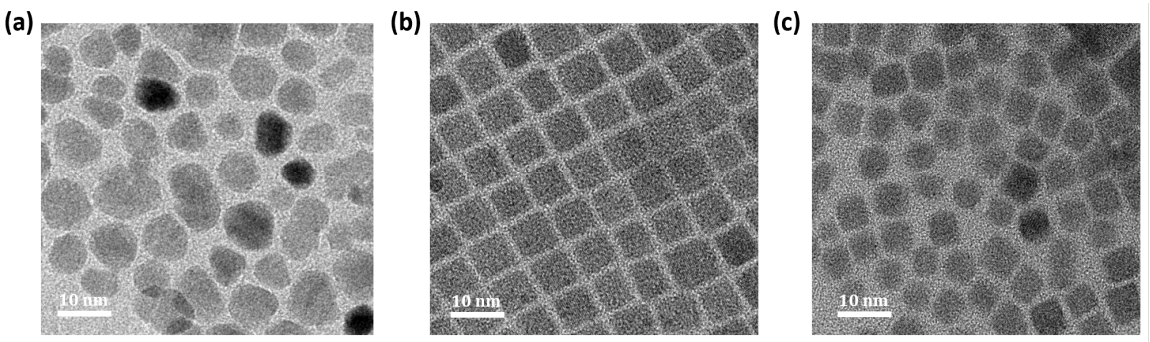

Figure 7. TEM images of (**a**) ZnO, (**b**) $CsPbBr_3$, and (**c**) the $CsPbBr_3$-ZnO mixture (1:0.015) in the film state.

Using AFM, the surface roughness of three different films—$CsPbBr_3$, ZnO, and the $CsPbBr_3$-ZnO mixture (1:0.015)—was evaluated (Figure 8). The analysis showed that the root mean square (RMS) roughness values were 3.92 nm for the $CsPbBr_3$ film, 4.14 nm for the ZnO film, and 4.59 nm for the $CsPbBr_3$-ZnO mixture (1:0.015) film. All films exhibited RMS values below 5 nm, resulting in a smooth surface. This will help suppress negative scattering effects that occur on the surface when fabricating multi-layered devices and enhance light conversion efficiency.

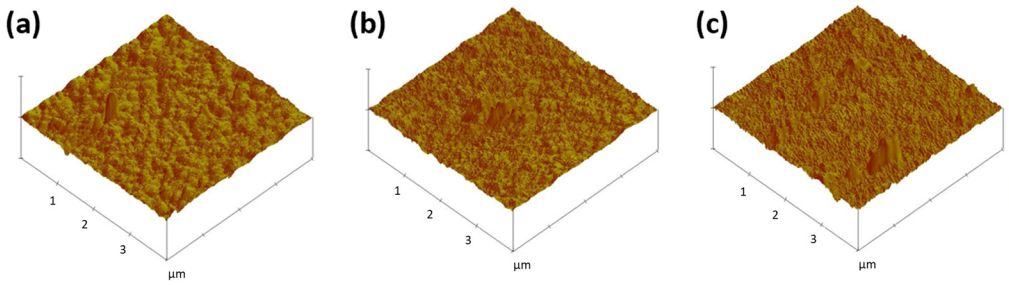

Figure 8. AFM images of (**a**) ZnO, (**b**) $CsPbBr_3$, and (**c**) the $CsPbBr_3$-ZnO mixture (1:0.015) in the film state.

4. Conclusions

We successfully fabricated thin films by dispersing zinc oxide with a size of 10 nm in a variety of compositions within $CsPbBr_3$ perovskite PL films to achieve a uniform composite structure. The resulting $CsPbBr_3$ films containing ZnO utilized the scattering effect of ZnO, which induced a relatively significant reflection of the incident light, leading to an enhancement in PL intensity. After investigating the optimal ratio of polar solvent commonly used for metal oxides, we established a weight ratio of 1:0.015 for ZnO and perovskite. The PL intensity increased by approximately 20% in the shaking mixture, and this improvement was attributed to the long delayed lifetime observed in the TRPL experiments. This study successfully demonstrates a method for forming a mixture of ZnO and perovskite without compromising the inherent characteristics of the perovskite. This approach can be utilized for the optimization of composite materials with various metal oxides of differing refractive indices and multiple perovskite materials, leading to enhanced light conversion efficiency in future developments.

Author Contributions: Conceptualization, H.K. and J.P.; methodology, N.K., H.K. and S.P. (Sunwoo Park); validation, S.P. (Sunwoo Park), S.P. (Sangwook Park) and H.L.; formal analysis, N.K. and H.K.; investigation, S.P. (Sunwoo Park) and H.L; resources, J.P.; writing—original draft preparation, N.K., H.K. and S.P. (Sunwoo Park); writing—review and editing, H.L and J.P.; visualization, N.K., H.K. and S.P. (Sangwook Park); supervision, J.P.; project administration, J.P.; funding acquisition, J.P. All authors have read and agreed to the published version of the manuscript.

Funding: This research was supported by the Basic Science Research Program through the National Research Foundation of Korea (NRF) funded by the Ministry of Education (2020R1A6A1A03048004). This work was partly supported by the GRRC program of Gyeonggi province [(GRRCKYUNGHEE2023-B01), Development of ultra-fine process materials based on the sub-nanometer class for the next-generation semiconductors]. This work was supported by the Technology Innovation Program (RS-2024-00423271, Development of mass production technology for high-quality perovskite light-emitting nanocrystal) funded By the Ministry of Trade, Industry & Energy (MOTIE, Korea).

Data Availability Statement: Data are contained within the article.

Conflicts of Interest: The authors declare no conflicts of interest.

References

1. Song, J.; Li, J.; Li, X.; Xu, L.; Dong, Y.; Zeng, H. Quantum Dot Light-Emitting Diodes Based on Inorganic Perovskite Cesium Lead Halides ($CsPbX_3$). *Adv. Mater.* **2015**, *27*, 7162–7167. [CrossRef] [PubMed]
2. Wang, Y.; Li, X.; Song, J.; Xiao, L.; Zeng, H.; Sun, H. All-Inorganic Colloidal Perovskite Quantum Dots: A New Class of Lasing Materials with Favorable Characteristics. *Adv. Mater.* **2015**, *27*, 7101–7108. [CrossRef]
3. Hu, F.; Zhang, H.; Sun, C.; Yin, C.; Lv, B.; Zhang, C.; Yu, W.W.; Wang, X.; Zhang, Y.; Xiao, M. Superior Optical Properties of Perovskite Nanocrystals as Single Photon Emitters. *ACS Nano* **2015**, *9*, 12410–12416. [CrossRef] [PubMed]
4. Kulbak, M.; Cahen, D.; Hodes, G. How Important Is the Organic Part of Lead Halide Perovskite Photovoltaic Cells? Efficient $CsPbBr_3$ Cells. *J. Phys. Chem. Lett.* **2015**, *6*, 2452–2456. [CrossRef] [PubMed]
5. Kim, Y.H.; Cho, H.; Heo, J.H.; Kim, T.S.; Myoung, N.S.; Lee, C.L.; Im, S.H.; Lee, T.W. Multicolored Organic/Inorganic Hybrid Perovskite Light-Emitting Diodes. *Adv. Mater.* **2015**, *27*, 1248–1254. [CrossRef]
6. Lin, C.C.; Yeh, S.Y.; Huang, W.L.; Xu, Y.X.; Huang, Y.S.; Yeh, T.H.; Tien, C.H.; Chen, L.C.; Tseng, Z.L. Using Thermally Crosslinkable Hole Transporting Layer to Improve Interface Characteristics for Perovskite $CsPbBr_3$ Quantum-Dot Light-Emitting Diodes. *Polymers* **2020**, *12*, 2243. [CrossRef]
7. Du, X.; Wu, G.; Cheng, J.; Dang, H.; Ma, K.; Zhang, Y.W.; Tan, P.F.; Chen, S. High-Quality $CsPbBr_3$ Perovskite Nanocrystals for Quantum Dot Light-Emitting Diodes. *RSC Adv.* **2017**, *7*, 10391–10396. [CrossRef]
8. Hua, J.; Deng, X.; Niu, C.; Huang, F.; Peng, Y.; Li, W.; Ku, Z.; Cheng, Y. bing A Pressure-Assisted Annealing Method for High Quality $CsPbBr_3$ Film Deposited by Sequential Thermal Evaporation. *RSC Adv.* **2020**, *10*, 8905–8909. [CrossRef]
9. Zhang, X.; Wang, F.; Zhang, B.B.; Zha, G.; Jie, W. Ferroelastic Domains in a $CsPbBr_3$ Single Crystal and Their Phase Transition Characteristics: An in Situ TEM Study. *Cryst. Growth Des.* **2020**, *20*, 4585–4592. [CrossRef]
10. Wang, H.C.; Bao, Z.; Tsai, H.Y.; Tang, A.C.; Liu, R.S. Perovskite Quantum Dots and Their Application in Light-Emitting Diodes. *Small* **2018**, *14*, 1702433. [CrossRef]
11. Xing, G.; Mathews, N.; Lim, S.S.; Yantara, N.; Liu, X.; Sabba, D.; Grätzel, M.; Mhaisalkar, S.; Sum, T.C. Low-Temperature Solution-Processed Wavelength-Tunable Perovskites for Lasing. *Nat. Mater.* **2014**, *13*, 476–480. [CrossRef] [PubMed]
12. Protesescu, L.; Yakunin, S.; Bodnarchuk, M.I.; Krieg, F.; Caputo, R.; Hendon, C.H.; Yang, R.X.; Walsh, A.; Kovalenko, M.V. Nanocrystals of Cesium Lead Halide Perovskites ($CsPbX_3$, X = Cl, Br, and I): Novel Optoelectronic Materials Showing Bright Emission with Wide Color Gamut. *Nano Lett.* **2015**, *15*, 3692–3696. [CrossRef] [PubMed]
13. Li, J.; Xu, L.; Wang, T.; Song, J.; Chen, J.; Xue, J.; Dong, Y.; Cai, B.; Shan, Q.; Han, B.; et al. 50-Fold EQE Improvement up to 6.27% of Solution-Processed All-Inorganic Perovskite $CsPbBr_3$ QLEDs via Surface Ligand Density Control. *Adv. Mater.* **2017**, *29*, 1603885. [CrossRef] [PubMed]
14. Yu, X.; Guo, J.; Mao, Y.; Shan, C.; Tian, F.; Meng, B.; Wang, Z.; Zhang, T.; Kyaw, A.K.K.; Chen, S.; et al. Enhancing the Performance of Perovskite Light-Emitting Diodes via Synergistic Effect of Defect Passivation and Dielectric Screening. *Nanomicro Lett.* **2024**, *16*, 205. [CrossRef]
15. Park, C.Y.; Choi, B. Enhanced Light Extraction from Bottom Emission OLEDs by High Refractive Index Nanoparticle Scattering Layer. *Nanomaterials* **2019**, *9*, 1241. [CrossRef]
16. Kim, S.; Kang, S.; Baek, S.; Song, J.; Mun, N.E.; Kwon, H.; Kwon, H.G.; Pu, Y.J.; Lee, T.W.; Yoo, S.; et al. Highly Thin Film with Aerosol-Deposited Perovskite Quantum Dot/Metal Oxide Composite for Perfect Color Conversion and Luminance Enhancement. *Chem. Eng. J.* **2022**, *441*, 135991. [CrossRef]
17. Das, A.; Basak, D. Efficacy of Ion Implantation in Zinc Oxide for Optoelectronic Applications: A Review. *ACS Appl. Electron. Mater.* **2021**, *3*, 3693–3714. [CrossRef]
18. Ramelan, A.H.; Wahyuningsih, S.; Munawaroh, H.; Narayan, R. ZnO Wide Bandgap Semiconductors Preparation for Optoelectronic Devices. *IOP Conf. Ser. Mater. Sci. Eng.* **2017**, *176*, 012008. [CrossRef]
19. Djuriić, A.B.; Ng, A.M.C.; Chen, X.Y. ZnO Nanostructures for Optoelectronics: Material Properties and Device Applications. *Prog. Quantum Electron.* **2010**, *34*, 191–259. [CrossRef]
20. Pradel, K.C.; Ding, Y.; Wu, W.; Bando, Y.; Fukata, N.; Wang, Z.L. Optoelectronic Properties of Solution Grown ZnO N-p or p-n Core-Shell Nanowire Arrays. *ACS Appl. Mater. Interfaces* **2016**, *8*, 4287–4291. [CrossRef]
21. Bhat, T.S.; Bhogale, S.B.; Patil, S.S.; Pisal, S.H.; Phaltane, S.A.; Patil, P.S. Synthesis and Characterization of Hexagonal Zinc Oxide Nanorods for Eosin-y Dye Sensitized Solar Cell. *Mater. Today Proc.* **2021**, *43*, 2800–2804. [CrossRef]

22. Chavan, R.D.; Wolska-Pietkiewicz, M.; Prochowicz, D.; Jędrzejewska, M.; Tavakoli, M.M.; Yadav, P.; Hong, C.K.; Lewiński, J. Organic Ligand-Free ZnO Quantum Dots for Efficient and Stable Perovskite Solar Cells. *Adv. Funct. Mater.* **2022**, *32*, 2205909. [CrossRef]
23. Jha, J.K.; Santos-Ortiz, R.; Du, J.; Shepherd, N.D. Semiconductor to Metal Transition in Degenerate ZnO: Al Films and the Impact on Its Carrier Scattering Mechanisms and Bandgap for OLED Applications. *J. Mater. Sci. Mater. Electron.* **2014**, *25*, 1492–1498. [CrossRef]
24. Ding, M.; Guo, Z.; Zhou, L.; Fang, X.; Zhang, L.; Zeng, L.; Xie, L.; Zhao, H. One-Dimensional Zinc Oxide Nanomaterials for Application in High-Performance Advanced Optoelectronic Devices. *Crystals* **2018**, *8*, 223. [CrossRef]
25. Wibowo, A.; Marsudi, M.A.; Amal, M.I.; Ananda, M.B.; Stephanie, R.; Ardy, H.; Diguna, L.J. ZnO Nanostructured Materials for Emerging Solar Cell Applications. *RSC Adv.* **2020**, *10*, 42838–42859. [CrossRef] [PubMed]
26. Yu, L.; Li, Z. Synthesis of $Zn_xCd_{1-x}Se$@ZnO Hollow Spheres in Different Sizes for Quantum Dots Sensitized Solar Cells Application. *Nanomaterials* **2019**, *9*, 132. [CrossRef]
27. Luo, L.; Lv, G.; Li, B.; Hu, X.; Jin, L.; Wang, J.; Tang, Y. Formation of Aligned ZnO Nanotube Arrays by Chemical Etching and Coupling with CdSe for Photovoltaic Application. *Thin Solid. Film. Film.* **2010**, *518*, 5146–5152. [CrossRef]
28. Rama Krishna, C.; Kang, M. Improving the Photovoltaic Conversion Efficiency of ZnO Based Dye Sensitized Solar Cells by Indium Doping. *J. Alloys Compd.* **2017**, *692*, 67–76. [CrossRef]
29. Nenna, G.; De Girolamo Del Mauro, A.; Massera, E.; Bruno, A.; Fasolino, T.; Minarini, C. Optical Properties of Polystyrene-ZnO Nanocomposite Scattering Layer to Improve Light Extraction in Organic Light-Emitting Diode. *J. Nanomater.* **2012**, *2012*, 319398. [CrossRef]
30. Kwon, H.; Park, S.; Kang, S.; Park, S.; Pu, Y.J.; Park, J. Three-Color White Electroluminescence Emission Using Perovskite Quantum Dots and Organic Emitters. *Appl. Surf. Sci.* **2022**, *588*, 152875. [CrossRef]
31. Lee, G.; Lee, S.Y.; Park, S.; Jang, S.H.; Park, H.K.; Choi, I.; Park, J.; Choi, J. Highly Effective Surface Defect Passivation of Perovskite Quantum Dots for Excellent Optoelectronic Properties. *J. Mater. Res. Technol.* **2022**, *18*, 4145–4155. [CrossRef]
32. Wolska-Pietkiewicz, M.; Jędrzejewska, M.; Tokarska, K.; Wielgórska, J.; Chudy, M.; Grzonka, J.; Lewiński, J. Towards Bio-Safe and Easily Redispersible Bare ZnO Quantum Dots Engineered via Organometallic Wet-Chemical Processing. *Chem. Eng. J.* **2023**, *455*, 140497. [CrossRef]
33. Xing, J.; Yan, F.; Zhao, Y.; Chen, S.; Yu, H.; Zhang, Q.; Zeng, R.; Demir, H.V.; Sun, X.; Huan, A.; et al. High-Efficiency Light-Emitting Diodes of Organometal Halide Perovskite Amorphours Nanoparticles. *ACS Nano* **2016**, *10*, 6623–6630. [CrossRef] [PubMed]